External Phase Shifting Tuning Mechanism in a Miniature Pulse Tube Cryocooler Using a Semi-Active Electromagnetic Damping System

Y. Greenberg and G. Grossman

Technion – Israel Institute of Technology
Haifa, Israel 32000

ABSTRACT

A semi-active electromagnetic damping mechanism was developed to externally control the phase shift and amplitude at the hot end of a pulse tube (PT) cryocooler. The semi-active phase shift (SAPS) mechanism was designed, built and tested, and included a voice coil suspended on a silicon diaphragm and a flexural bearing. The development included theoretical calculations, numerical optimization using SAGE®, flexure bearing optimization and development, off-the-shelf voice coil selection and modal simulations of the entire system using ANSYS® finite element software.

The goal was to obtain the optimum phase shift between pressure and flow rate and thus reach the optimal cryocooler performance. During experiments, a stick-slip phenomenon inherent to the voice coil influenced the cryocooler performance, and the lowest temperature observed in the experiments was 225K (without vacuum in the containing chamber) at 100 Hz operational frequency. However, the results show that the system was capable of externally tuning the cold end temperature, and provided a proof of concept for the application of external phase shift and amplitude tunable mechanism.

INTRODUCTION

The pulse tube (PT) cryocooler, based on the Stirling thermodynamic cycle, operates with oscillating pressure and mass flow and has no moving displacer at the cold end. The main advantage of such a cryocooler involves longer life-times together with higher efficiency, essential for operational systems with high reliability requirements.

It was investigated and proved that the optimal phase relationship between the flow and pressure in a pulse tube cryocooler is that in which the flow at the regenerator midpoint is nearly in phase with the pressure, which infers a flow-to-pressure phase difference at the warm end, typically around -60 degrees [1].

One of the most common passive methods of the flow-to-pressure phase shifting involves the use of an inertance tube (IT) combined with a reservoir. When attempting to miniaturize this type of cryocooler, the efficiency degrades since the resistive fluid impedance increases rapidly with decreasing size. In previous research, an innovative phase shifter using an IT filled with liquid, and separated by a sealed metallic diaphragm has been implemented and tested [2]. This compact cryocooler operated at 8-80K and validated the device in operation. In order to optimize perfor-

Cryocoolers 21, edited by R.G. Ross, Jr., J.R. Raab and S.D. Miller

mance, the IT was filled with different types of liquids. Other research [3] used a warm expander as an active mechanical phase shifter for pulse tube cryocoolers. That work used a linear compressor (pressure oscillator) at the warm side of the pulse tube cryocooler and thus controlled the phase shift between pressure and mass flow. This implementation has improved cryocooler performance but involved the requirement for extra electrical energy.

Previous research by Sobol and Grossman [4] proposed to construct a passively linear oscillating mass-damper mechanism, as a solution for flow-to-pressure phase shifting to replace the use of an inertance tube. This phase shifting device was implemented in a miniature cryocooler (MTSb) constructed in our laboratory [5], originally using an inertance tube. Much like the IT/reservoir, that device implementation was designed for a specific cold end temperature and a cycle operating frequency. In addition, mechanical tolerances affected the device performance.

The above research was an improved implementation of an earlier study performed by Radchenko and Grossman [6], which also dealt with a passive mechanical device for phase shifting in a pulse tube cryocooler. The system included an oscillating mass, flexure bearings and damping whose source was an oscillating gas in a precise clearance gap (20 μm). The damping implementation was significantly affected by manufacturing inaccuracies, which added parasitic friction between piston and cylinder. As a result, the cryocooler was unable to reach the theoretical cold temperatures and efficiency was relatively low.

In the current research, the passive linear oscillating mass-damper mechanism, which was previously developed at the Rechler Cryogenic Laboratory at the Technion [7], was replaced by the SAPS mechanism. The proposed phase shifting mechanism consists of a 5 mm effective diameter silicon diaphragm piston attached to a voice coil suspended on a flexure bearing. The acoustic oscillations generated in the PT displace the voice coil axially and thus create an electrical current through its wires, similar to the operation of an alternator in a thermoacoustic engine cycle [8]. The main design parameters included a total oscillating mass of 40 gr, 10,100 N/m overall axial stiffness and external adjustable resistor (10 - 30 Ohm) and inductor (2 - 17 mH) to control the mechanism overall damping and axial stiffness.

PRINCIPLE OF OPERATION

Figure 1 demonstrates the proposed external phase control mechanism schematically. The mechanism includes an oscillating mass m, with a cross section A. The total warm control space is partitioned into two volumes: the front volume V_f and the inside volume V_i. The oscillating mass serves as a piston separating the two volumes. The absolute pressures within those volumes are P_f and P_i, respectively. There exists an average uniform pressure P_0 in the system that is equal to the filling pressure of the cryocooler. The pulse tube component is connected through a transfer line to the piston front volume, where in that volume a proper flow-to-pressure phase and amplitude must be created to obtain an efficient cryocooler cycle.

The main part of the mass m is a coil displaced in a linear motion, driven by an oscillating pressure force. The mass is supported axially by a mechanical spring with stiffness k. Since the piston is intended to be implemented as an elastomeric diaphragm, a hysteretic damping coefficient η characterizing it is considered. A coil moving inside a magnetic field will provide an opposing Lorentz force to the oscillating driving pressure force.

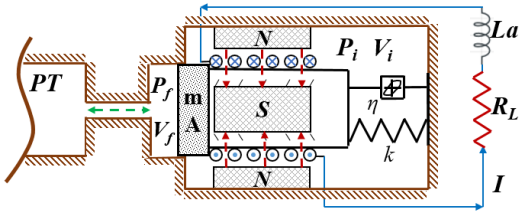

Figure 1. Schematic description of proposed external phase control mechanism

The opposing Lorentz force, which is dependent on the current I, will provide a certain induced damping and stiffness on the oscillating mass within the system. The induced damping and stiffness can therefore be tuned by changing the current through an external coil with inductance L_a and an external load resistor with resistance R_L.

Principal equations

To obtain the pressure-to-flow phase and amplitude, we separate the proposed system into acoustical, mechanical and electrical disciplines. Solving each discipline will provide a system of equations and parameters. For small piston displacements, the force factor Bl, and voice coil inductance L_{vc} are assumed to be constant for *NdFeB* magnets [9].

The electrical discipline can be solved by applying Kirchhoff's voltage law (KVL):

$$\varepsilon = Bl\frac{dx}{dt} = R_T i(t) + L_T \frac{di}{dt} \tag{1}$$

where ε is the induced EMF (electromotive force) caused by the motion of the voice coil. The total electrical resistance is $R_T = R_{vc}+R_L$ and the total electrical inductance $L_T = L_{vc}+L_a$. R_{vc}, L_{vc} are the voice coil's internal electrical resistance and inductance, respectively. R_L and L_a are the external tunable electrical resistance and inductance, respectively.

The free body force diagram of the investigated research system described in Figure 1 is shown in Figure 2. Since the damping concept is implemented using an electromagnetic damper, the viscous damping was neglected. In addition, it is assumed in the developed theoretical model that no external friction exists.

Applying Newton's 2nd law, the sum of forces ΣF_x acting on the piston along the x direction is:

$$F_{Acoustic}(t) - \left(\frac{k_{ms}\eta}{\omega}\right)\frac{dx}{dt} - \left[k_{ms}+k_m+k_{gi}\right]x(t) - F_B(t) = m\frac{d^2x}{dt^2} \tag{2}$$

where $F_{Acoustic}$ is the internal oscillating acoustic driving force from the Pulse Tube, F_B is the Lorentz force described earlier in this chapter, k_{gi} is the gas stiffness available from the inside gas pressure P_i. k_m is the mechanical elastic stiffness of the SS flexure bearing, k_{ms} is the stiffness of the hyper-elastic silicon material which has a hysteretic damping coefficient η at a working frequency ω. A hysteretic damping is a type of dissipation that is a function of friction within the material. m is the total oscillating mass.

The acoustic driving force $F_{Acoustic}$ is described as the pressure difference on the diaphragm piston effective area:

$$F_{Acoustic}(t) = \left[P_f(t) - P_i(t)\right]A = p(t)A = P_1\cos(\omega t)A \tag{3}$$

Lorentz force is defined as:

$$F_B(t) = Bli(t) \tag{4}$$

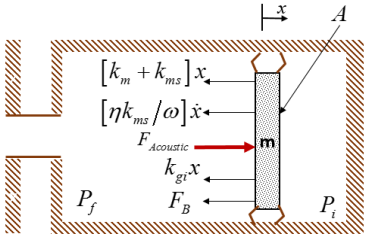

Figure 2. Free Body Diagram of the investigated oscillating mass

The internal volume gas stiffness k_{gi} can be calculated using the conservation of mass equation within the adiabatic internal volume V_i, under the assumptions of small pressure ratios [10].

We will solve the systems of Eqs. (1) and (4) with two unknowns: R_T and L_T, using the Laplace Transform approach. The travel-to-pressure transfer function is obtained in order to calculate the travel-to-pressure phase and piston amplitude:

$$G(s)=\frac{X(s)}{P(s)}=\frac{A}{ms^2+\dfrac{(Bl)^2 s}{R_T+L_T s}+\dfrac{\eta k_{ms}}{\omega}s+\left(k_{ms}+k_m+k_{gi}\right)} \tag{5}$$

The solution for the travel-to-pressure phase is the following:

$$\theta=\angle G(j\omega)=\arctan\left[\frac{-\eta k_{ms}\left(R_T{}^2+L_T{}^2\omega^2\right)-(Bl)^2 R_T\omega}{\left(\left(k_{gi}+k_m+k_{ms}\right)-m\omega^2\right)\left(R_T{}^2+L_T{}^2\omega^2\right)+(Bl)^2 L_T\omega^2}\right] \tag{6}$$

The piston amplitude is the following:

$$\left|X(j\omega)\right|=\left[\frac{A\left|P(j\omega)\right|}{\sqrt{\underbrace{\left(\frac{(Bl)^2 R_T\omega}{R_T{}^2+L_T{}^2\omega^2}+\eta k_{ms}\right)^2}_{\text{Damping expression}}+\underbrace{\left(k_m+k_{ms}+k_{gi}-m\omega^2+\frac{(Bl)^2 L_T\omega^2}{R_T{}^2+L_T{}^2\omega^2}\right)^2}_{\text{Stiffness expression}}}}\right] \tag{7}$$

The magnetic damping and magnetic stiffness, obtained from Eq. 7 are therefore: $b_{mag}=(Bl)^2 R_T/\left(R_T{}^2+L_T{}^2\omega_0{}^2\right)$ and $k_{mag}=(Bl)^2 L_T\omega_0{}^2/\left(R_T{}^2+L_T{}^2\omega_0{}^2\right)$ respectively.

Setting the optimized flow-to-pressure phase (θ_0) and piston stroke x_1 as design criteria from SAGE® numerical optimization software, we obtain the solutions for R_T and L_T.

$$R_T=\frac{Bl^2\omega_0 x_1\cdot\left(AP_1\left|\cos(\theta_0)\right|\cdot\tan(\theta_0)-\eta k_{ms}x_1\right)}{\left[\begin{array}{l}x_1{}^2\left(\eta^2 k_{ms}{}^2+\left(k_{gi}+k_m+k_{ms}\right)^2-2m\omega_0{}^2\left(k_{gi}+k_m+k_{ms}\right)+m^2\omega_0{}^4\right)+\\+A^2P_1^2\left|\cos(\theta_0)\right|^2\left(1+\tan(\theta_0)^2\right)+\\+2AP_1x_1\left|\cos(\theta_0)\right|\left(k_{gi}+k_m+k_{ms}-\eta k_{ms}\tan(\theta_0)-m\omega_0{}^2\right)\end{array}\right]} \tag{8}$$

$$L_T=\frac{Bl^2x_1\cdot\left(mx_1\omega_0{}^2-x_1\left(k_{gi}+k_m+k_{ms}\right)-AP_1\left|\cos(\theta_0)\right|\right)}{\left[\begin{array}{l}x_1{}^2\left(\eta^2 k_{ms}{}^2+\left(k_{gi}+k_m+k_{ms}\right)^2-2m\omega_0{}^2\left(k_{gi}+k_m+k_{ms}\right)+m^2\omega_0{}^4\right)+\\+A^2P_1^2\left|\cos(\theta_0)\right|^2\left(1+\tan(\theta_0)^2\right)\\+2AP_1x_1\left|\cos(\theta_0)\right|\left(k_{gi}+k_m+k_{ms}-\eta k_{ms}\tan(\theta_0)-m\omega_0{}^2\right)\end{array}\right]} \tag{9}$$

An iterative optimization process was used by SAGE® in order to solve the cryocooler cycle under best performance, i.e., maximum cooling power [W]. The design goal was to maximize the cooling power by running the simulation with an optimal pressure ratio in the aftercooler, depending on the MTSb compressor characteristics**.** The results for b_{mag} and k_{mag} from SAGE® were then compared to the analytical results from Eqs (1)-(7) solved in MATLAB®, until a match was reached. Thus, the values of the total electrical resistance and inductance, R_T and L_T, Eq. (8) and (9), leading to this optimum performance, were obtained.

Table 1. Design criteria, inputs and goals

Inputs	Description	Parameter
SAGE®	Desired cold temperature [*K*]	T_c
	Travel amplitude [*m*]	x_1
	Travel-to-pressure phase [*deg*]	θ_0
	Pressure amplitude [*Pa*]	P_1
Operating point	Operational frequency [*Hz*]	ω_0
	Filling pressure [*Pa*]	P_0
Mechanical design	Mechanical stiffness [*N/m*]	k_m+k_{ms}
	Hysteresis damping [-]	η
	Initial internal volume [m^3]	V_{i0}
	Piston effective area [m^2]	A
	Reciprocating mass [*kg*]	m
	Voice coil force factor [*N/A*]	Bl

Design criteria

Table 1 describes the design criteria, inputs and goals for the current Semi-Active phase shifting system.

CAD Model

Figure 3 shows a general view of the MTSb cryocooler with an additional chamber cover added to accommodate the larger SAPS assembly size. Vacuum is created inside the chamber to improve the cryocooler operating conditions by isolating it from the environment. The sealed external connector serves to monitor the data from the temperature and pressure sensors within the cryocooler. In addition, it would be used to connect the external resistor and inductor to tune the damping and stiffness of the SAPS to control the phase shifting and piston amplitude for optimal cycle conditions. The compressor is connected through the inlet line. This cryocooler would now be referred to as MTSb-SAPS cryocooler (SAPS stands for Semi-Active Phase Shift). Figure 5 shows a cross section of the preliminary CAD model, and Figure 4 shows a detailed view of the dynamic oscillating SAPS components.

Since the working frequency is 100 Hz, it is important to make sure that there are no parasitic resonance modes around this frequency which might hinder the SAPS performance. Therefore, a

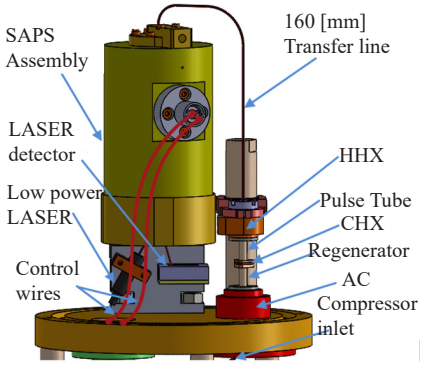

Figure 3. Detailed description of the MTSb cryocooler with the semi-active phase shift mechanism assembly

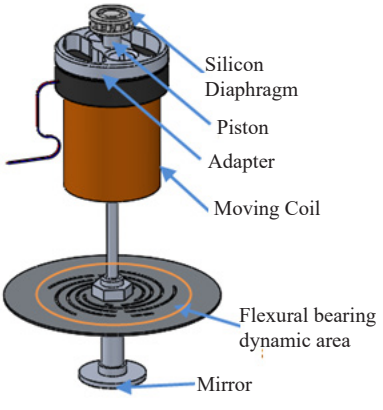

Figure 4. Oscillating SAPS components

Table 2. MTSb-SAPS cryocooler parameters

	Connector	AC	Regenerator	Cold HX	Pulse Tube	Hot HX	Transfer line
Length [mm]	70	2	12	0.4	14	0.6	160
Inner Diameter [mm]	1.1	4	3.8	4	3.8	4	0.7

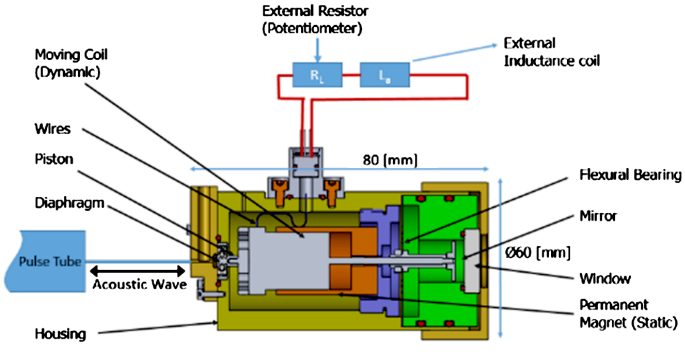

Figure 5. Cross section of the SAPS mechanism CAD design

modal analysis was performed. The silicon diaphragm equivalent Young modulus of 0.6581 MPa has been determined by iterative static simulations.

The first two modes were 80 Hz, 220 Hz. From this analysis we expect not to have any parasitic resonance modes during system operation at 100 Hz.

Experimental setup

An optical measurement system was used for measuring the oscillating SAPS piston displacement and is schematically described in Figure 6. A laser beam of 0.9 mW with a wavelength of 655 μm passed through a borosilicate glass window, and reflected back to a PSD from a reflective surface attached to the far side of the piston. The PSD work principle is based on a p-n junction which produces current and voltage which depend on the location of the laser beam position. The output voltage signal is then collected by a data acquisition software.

Figure 7 shows the MTSb-SAPS external electrical circuit assembly. The tunable resistor is connected in series with the inductor to the voice coil wires.

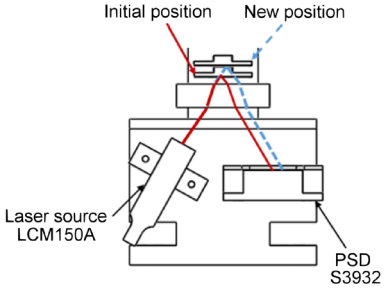

Figure 6. Optical piston displacement schematics

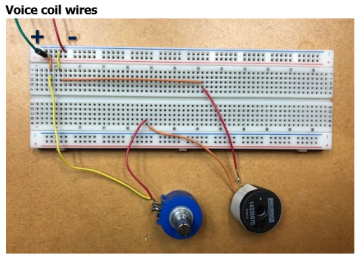

Figure 7. MTSb-SAPS electrical circuit assembly

Table 3. SAGE® inputs

Description	Parameter	Value
Working frequency	ω_0	100 Hz
Pressure ratio in the aftercooler	P_r	1.3
Filling pressure	P_0	4 MPa
Total measured mechanical stiffness	$k_{tm}=k_m+k_{ms}$	10,114 N/m
Hysteretic damping coefficient	η	0.1
Mass	m	40 gr
Effective Piston diameter	D_{eff}	5 mm
Transfer line length	L_f	160 mm
Cold temperature s (Design criteria)	Tcold	100…240 K

RESULTS AND DISCUSSION

Numerical and analytical results

Table 3 describes the design parameters of the MTSb-SAPS cryocooler. The design criterion is the cold temperature Tcold, since one would want to set the Tcold temperature to a suitable cryocooler's load at specific operating conditions.

Figure 8 shows the analytical calculated piston stroke at each frequency, with the displacement-to-pressure phase. The desired external resistance and inductance at each Tcold temperature were solved and are described in Figure 9.

Experiment results

In order to test how the change in the external electrical circuit load affects the cryocooler cooling performance, a fast transition experiment between closed and open electrical circuit was conducted. The closed circuit resistance and inductance are in fact the voice coil internal electrical parameters + wires: 8 Ohm and 2 mH respectively. In Figure 10 the cryocooler ran for 90 seconds until it reached steady state at ~ 240K in a closed circuit configuration. The electrical circuit was then opened and a rapid change in temperature was measured. This experiment proved that tuning the external electrical components influenced the cryocooler performance.

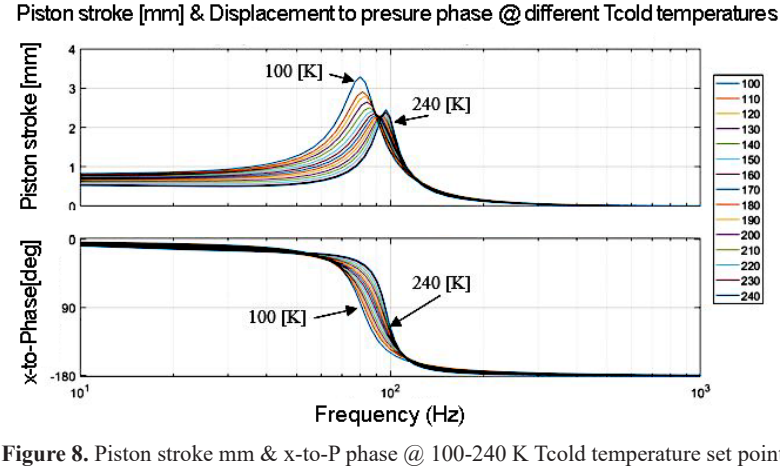

Figure 8. Piston stroke mm & x-to-P phase @ 100-240 K Tcold temperature set point

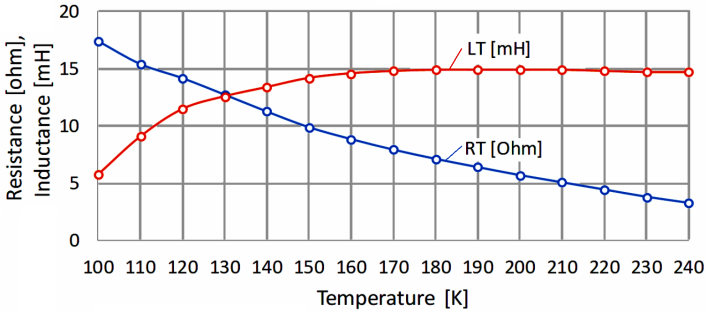

Figure 9. Optimization results: total resistance & inductance versus Tcold temperature.

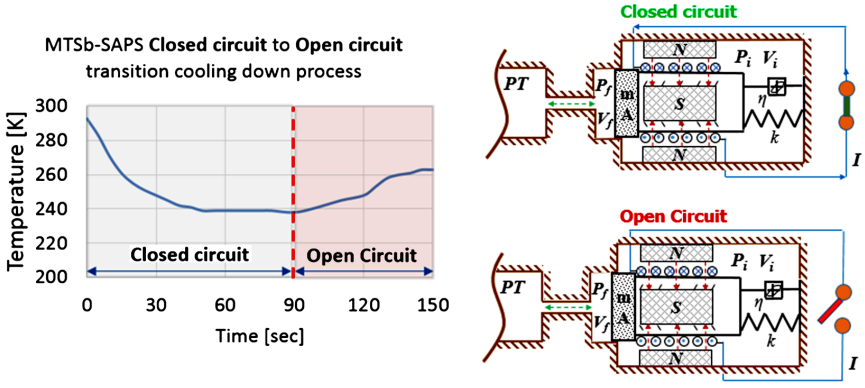

Figure 10. Closed circuit to Open circuit transition

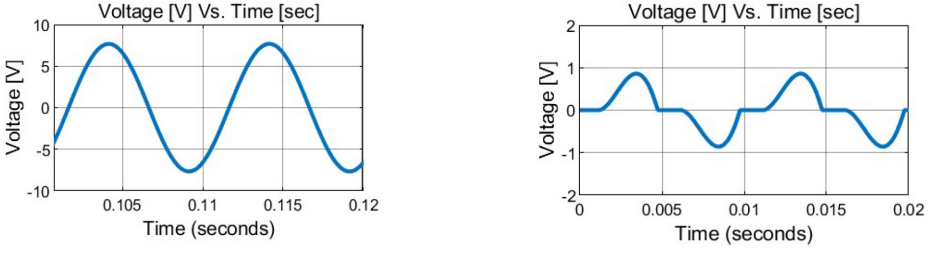

Figure 11. Calculated voice coil generated voltage before (left) and after (right) applying stick-slip model for RT = 17.4 Ohm, LT = 6 mH

Figures 10-12 show that the analytical with friction model and measured x-to-P phase resulted in ~40° shift from the theoretical simulation without friction for similar resistance R_T, and inductance L_T, described in Figure 8. In conclusion, friction was indeed a source of energy loss in the SAPS mechanism, caused phase shift and decreased piston amplitude which affected the mass flow at the warm end of the cryocooler and thus decreased the mass flow at the cold end, which possibly degraded the minimum Tcold temperature the cryocooler could reach.

The goal of this work has been to prove that an external fine-tuning phase shift implementation can internally affect the cryocooler flow-to-pressure phase shift and piston amplitude. Although

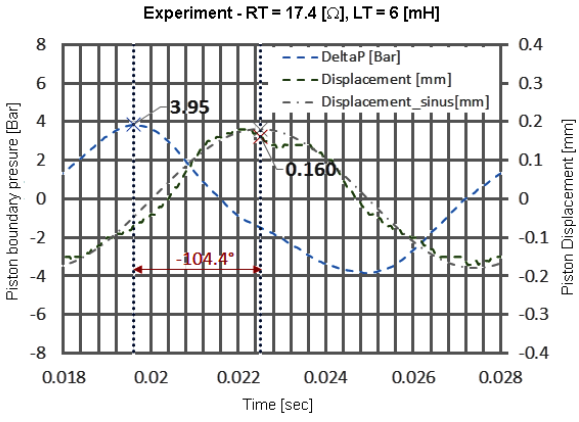

Figure 12. Measured x-to-P phase and displacement amplitude for RT=17.4 Ohm, LT=6 mH

the MTSb-SAPS Tcold temperature is not as low as demonstrated in the MTSa-IT cryocooler, the external phase shift tuning can still be investigated.

Since the friction phenomenon mentioned above affected the mass flow in the system, it was difficult to test the phase shift mechanism under theoretical resulting resistance and inductance described in Figure 9 for low Tcold temperatures. Nevertheless, 20 set points of experiments were tested in order to investigate how the external tuning mechanism affected the pulse tube Tcold temperature. Each set point was run for 5 times in order to obtain an average temperature with ±1K tolerance. The results are shown in Figure 13.

The tuning was conducted in an open loop, meaning the resistor and inductor were changed with no closed-loop control on the desired Tcold temperature. In order to prevent overshoots by on-line tuning, the resistor and inductor were tuned while the cryocooler was turned off.

SUMMARY AND CONCLUSIONS

A proof of concept for the application of external phase shift and amplitude tunable mechanism was demonstrated. The SAPS mechanism was designed, constructed, assembled and experimented with. That included diaphragm design and molding process, and flexure bearing optimization. With most data sets there is a good correlation between analytical and experimental results, with an average of 10% relative error for the piston amplitude and 5% relative error for the flow-to-pressure phase.

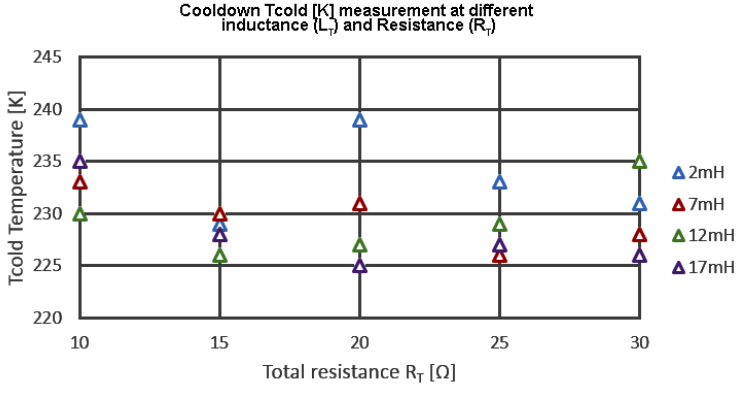

Figure 13. Experiment Tcold temperature vs. total resistance and inductance

Unfortunately, temperatures reached in the experiments (~230K) were higher than were supposed to be (~150K) as demonstrated earlier with the current PT MTSa-IT cryocooler. The reasons for disagreement with analytical and experiment simulations may be the stick-slip phenomenon observed and measured during the cryocooler runs. This phenomenon is caused by high friction between the dynamic (coil) and static (magnet) components of the voice coil. This phenomenon lowers the piston balance significantly. Decreasing the piston displacement affects the volumetric flow at the hot end, and thus affects different components in the PT cryocooler. A slight imbalance in the oscillating assembly may cause non-linear motion due to non-uniform friction caused by different contact points at each period.

A custom tailor-made voice-coil design may improve the MTSb-SAPS cryocooler. The design should implement a voice coil with a high force factor value, together with low internal resistance and inductance, and minimum friction. Further if practical, it is desired to implement a compact design, in order to decrease the system size.

ACKNOWLEDGMENT

The generous financial support of the Rechler Family, MAFAT and the Technion is gratefully acknowledged.

REFERENCES

1. R. Radebaugh, “Pulse Tube Cryocoolers,” *Low temperature and cryogenic refrigeration*, Dordrecht, The Netherlands, Kluwer Academic Publishers, 2003, pp. 415-434.
2. C. Ivan, D. Jean-Marc, D. Christophe and A. Jérôme, “Innovative phase shifter for pulse tube operating below 10K,” *Cryogenics,* vol. 78 (2016), pp. 89-95.
3. M. Lewis, P. Bradley and R. Radebaugh, “Experiments with linear compressors for phase shifting in pulse tube crycoolers,” *AIP Conference Proceedings,* vol. 1434, no. 1 (2012).
4. S. Sobol and G. Grossman, “Diaphragm-Type Mechanism for Passive Phase Shifting in Miniature PT Cryocooler,” *Cryocoolers 19,* ICC Press, Boulder, CO (2016), pp. 219-228.
5. S. Sobol, Y. Katz and G. Grossman, “A study of a miniature in-line pulse tube cryocooler,” *Cryocoolers 16,* ICC Press, Boulder, CO (2011), pp. 87-95.
6. D. Radchenko and G. Grossman, “Passive Mechanical Device for Phase Shifting in a Pulse Tube Cryocooler,” *Cryocoolers 19,* ICC Press, Boulder, CO (2016), pp. 201-210.
7. S. Sobol and G. Grossman, “Miniature PT Cryocooler Activated by Resonant Piezo electric Compressor and Passive Warm Expander,” *IOP Conference Series, Material Science and Engineering,* Vols. 012141/1-8 (2017), p. 278.
8. D. Sun, K. Wang, X. Zhang, Y. Guo, Y. Xu and L. Qiu, “A traveling-wave thermoacoustic electric generator with a variable electric R-C load,” *Applied Energy,* vol. 106 (2013), pp. 377-382.
9. A. Novak and B. Merit, “Magnet-only loudspeaker motors: linear behavior theory vs. Nonlinear measurements,” *Acoustics*, Nantes, France, (2012).
10. R. Radebaugh, “A Review of Pulse Tube Refrigeration,” *Fast R.W. (eds) Advances in Cryogenic Engineering,* vol. 35 (1990), pp. 1191-1205.
11. A. Jomde, A. Anderson, V. Bhojwani, F. Kharadi and S. Deshmukh, “Parametric Analysis of Flexure Bearing for Linear Compressor,” *Materials Today: Proceedings,* vol. 4 (2017), pp. 2478-2486.